

Jonathan A. Black¹

Centrifuge Modelling With Transparent Soil and Laser Aided Imaging

Reference

Black, Jonathan A., "Centrifuge Modelling With Transparent Soil and Laser Aided Imaging," *Geotechnical Testing Journal*, Vol. 38, No. 5, 2015, pp. 631–644, doi:10.1520/GTJ20140231. ISSN 0149-6115

ABSTRACT

Transparent synthetic soils have been developed as a soil surrogate to enable internal visualization of geotechnical processes in physical models. While significant developments have been made to enhance the methodology and capabilities of transparent soil modelling, the technique is not yet exploited to its fullest potential. Tests are typically conducted at 1 g in small bench size models, which invokes concerns about the impact of scale and stress level observed in previously reported work. This paper recognized this limitation and outlines the development of improved testing methodology whereby the transparent soil and laser aided imaging technique are translated to the centrifuge environment. This has a considerable benefit such that increased stresses are provided, which better reflect the prototype condition. The paper describes the technical challenges associated with implementing this revised experimental methodology, summarizes the test equipment/systems developed, and presents initial experimental results to validate and confirm the successful implementation and scaling of transparent soil testing to the high gravity centrifuge test environment. A 0.6 m wide prototype strip foundation was tested at two scales using the principle of "modelling of models," in which similar performance was observed. The scientific developments discussed have the potential to provide a step change in transparent soil modelling methodology, crucially providing more representative stress conditions that reflect prototype conditions, while making a broader positive contribution to physical modelling capabilities to assess complex soil–structure boundary problems.

Keywords

transparent soil, centrifuge, shallow foundation, physical modelling, modelling of models

Manuscript received September 30, 2014; accepted for publication March 16, 2015; published online April 15, 2015.

¹ Senior Lecturer & Director, Department of Civil and Structural Engineering, Centre for Energy and Infrastructure Research Centre, Univ. of Sheffield, Sheffield, S1 3JD, UK, e-mail: j.a.black@sheffield.ac.uk

Nomenclature

ac	= alternating current
B	= foundation width
cP	= viscometer in units of centipoises
c_u	= undrained shear strength
c_v	= coefficient of consolidation
dc	= direct current
DIC	= digital image correlation
f	= focal length
fps	= frames per second
g	= gravitational acceleration (9.81m/s^2)
h_m	= model height (m is subscript - Fig. 2)
h_p	= prototype height (p is subscript - Fig. 2)
MM	= multimode optic fiber cable
m_v	= coefficient of compressibility
n	= centrifuge acceleration scale
NA	= numerical aperture
q	= foundation stress
r	= radius
s	= foundation settlement
SLR	= single lens reflex
SM	= singlemode optic fiber cable
V	= volt
W	= watt
z	= depth
ϕ	= angle of shearing resistance
λ	= wavelength
ω	= angular velocity (ω)
v	= foundation installation velocity

Introduction

PHYSICAL MODELLING IN GEOTECHNICS

A wide range of visualization techniques have been developed within the field of geotechnical engineering to provide enhanced understanding of soil–structure interaction and collapse behavior in physical model tests. Plane strain modelling, where a geotechnical structure is viewed in half space symmetry through a viewing window, is a well-established and accepted geotechnical testing methodology. Soil behavior is observed using digital photography and digital image correlation (DIC) methods to provide an insight of displacement mechanics. [White et al. \(2003\)](#) developed an in-house code for image correlation referred to as “GeoPIV” based on DIC that utilizes variation in soil texture for tracking soil displacement in geotechnical application. Modern DIC methodology is an advancement on previously established imaging techniques such as stereo-photogrammetry ([Butterfield et al. 1970](#);

[Andrawes and Butterfield 1973](#)) and computer based image processing ([Taylor et al. 1998](#)).

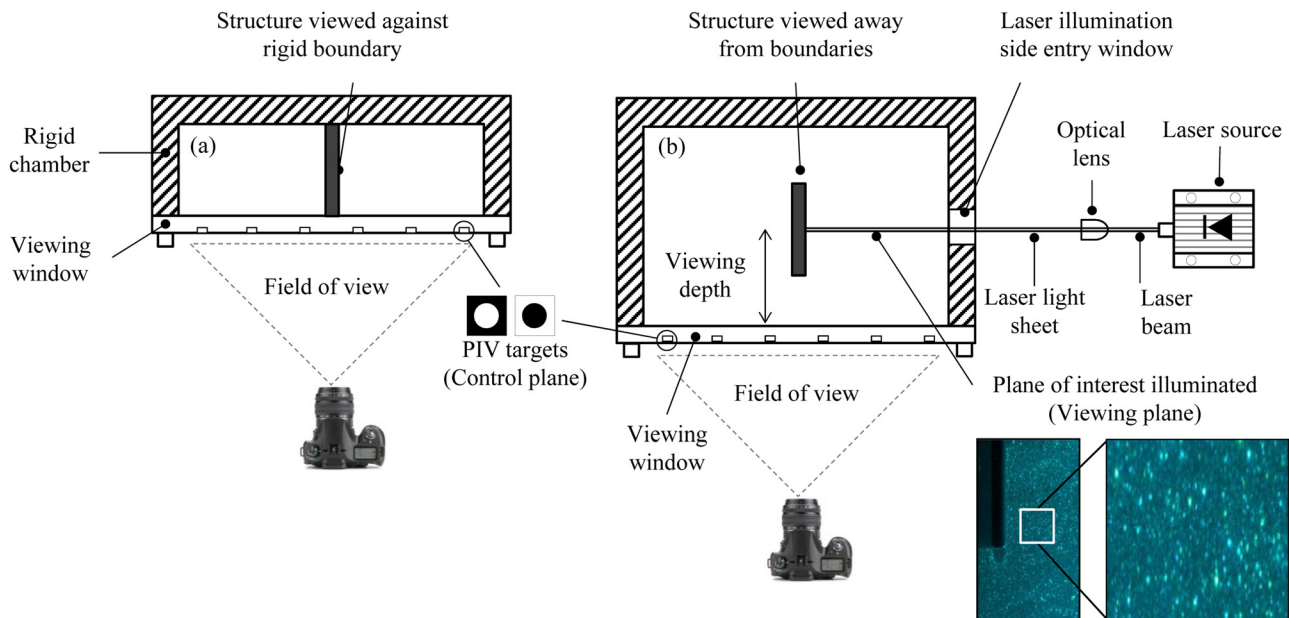
While this represents the current state-of-the-art for laboratory physical modelling, several limitations are inherent with the plane strain test configuration; for example: (i) measurements are restricted to the single plane exposed on the viewing window, (ii) interface friction along the viewing boundary surface influences the displacement behavior, (iii) geometrical simplification of the geostructure is necessary whereby models are restricted to being planar or having a line of symmetry, (iv) realistic construction processes (i.e., rotational installation) cannot be replicated against the rigid boundary viewing window, and (v) an inability to visualize internal soil displacements prevents enhanced understanding of complex 3D soil–structure interaction problems (**Fig. 1**). In this respect, internal sensors are frequently embedded within a model to capture spatial measurement of stress and pore pressure; however, this has an undesirable impact as it generates compliance errors and alters the ground stress profile in the soil continuum.

TRANSPARENT SOIL MODELLING

To overcome some of the aforementioned limitations, researchers developed translucent or transparent synthetic media as a soil surrogate, referred to as “transparent soil,” to enable internal visualization of geotechnical processes in physical model tests. Transparent soil consists of an aggregate and a matched refractive index fluid that when saturated enable internal visualization within the soil volume. This is beneficial as it enables the opportunity to observe a geostructure that is placed within the middle of a test chamber, thereby reducing boundary effects and the need for geometrical simplification of complex structures. Early experiments in transparent soil adopted back illumination to silhouette embedded target markers to capture the mechanical response of the soil and a geostructure ([Gill 1999](#); [McKelvey 2002](#); [McKelvey et al. 2004](#)); however, this was superseded by laser aided imaging in conjunction with DIC (**Fig. 1**). Recent works using this approach relate to model piles ([Iskander et al. 2002a](#)), shallow foundations ([Liu et al. 2002](#); [Iskander and Lui 2010](#)), tunnel induced settlements ([Ahmed and Iskander 2010](#)), helical screw piles ([Stanier et al. 2013](#)), stone column group behavior ([Kelly 2013](#)), soil plugging in tubular piles ([Black 2012a](#); [Forlati and Black 2014](#)), and sample disturbance effects during tube sample recovery ([Black 2012b](#)).

Other complementary work in the field has sought to increase the technical capabilities of transparent soil modelling by (i) evaluating and understanding the material properties ([Sadek et al. 2002](#); [Iskander et al. 2002a](#)), (ii) developing image capture and enhancement methods ([Gill and Lehane 2001](#); [Iskander et al. 2002b](#); [Sadek et al. 2003](#), [Hird et al. 2008](#); [Stanier et al. 2012](#); [Black and Take 2015](#)), increased (iii) multi-plane image reconstruction to understand complex 3D soil–structure interaction problems ([Iskander and Lui 2010](#); [Kelly 2013](#)). An

FIG. 1 Physical modelling methods: (a) plane strain modelling and (b) transparent soil non-intrusive modelling.



overall summary of the development of transparent soil and recent works was reported by [Iskander \(2010\)](#).

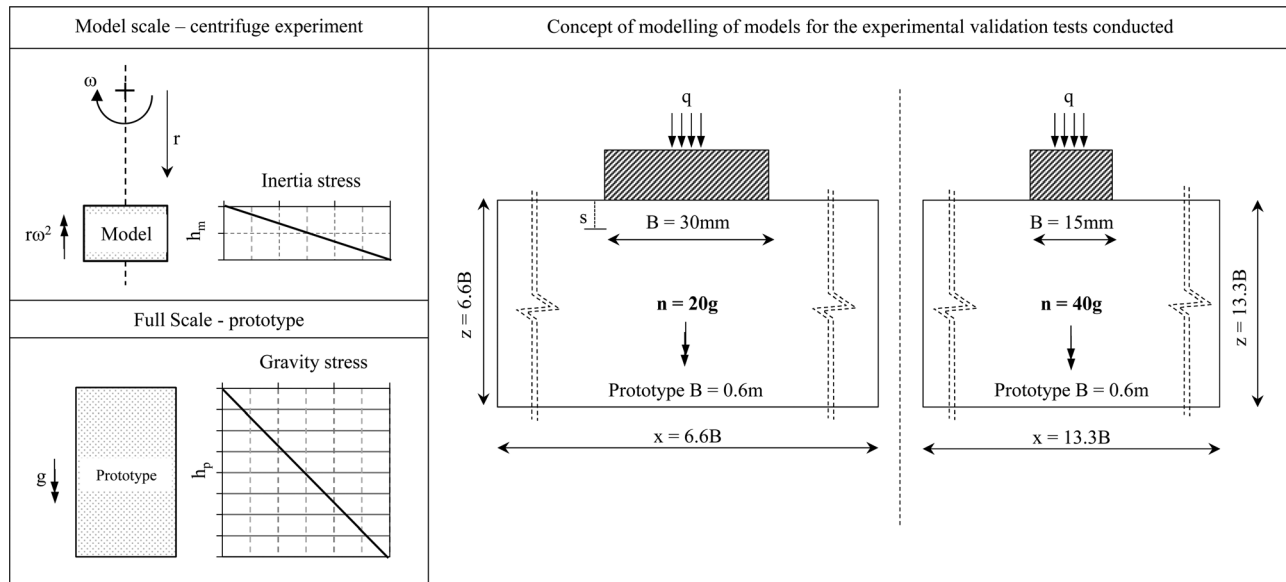
Limitations of Transparent Soil Modelling Capabilities

While significant developments have been made to enhance the methodology and capabilities of transparent soil modelling, the technique is not yet exploited to its fullest potential. Tests are conducted at small bench scale; however, unlike other forms of 1 g modelling, several shortcomings still persist: (i) the test configuration is complex and requires a laser illumination source which commands strict health and safety protocols, (ii) test chambers are typically fabricated from Perspex to enable the laser light sheet to penetrate the soil perpendicular to the front viewing window, which restricts the ability to provide increased vertical boundary stresses, and (iii) low optical transparency of the soil can limit the test chamber geometry such that containers of 100 by 100 mm plan area are frequently reported in literature.

These points invoke concerns about the impact of scale and boundary conditions observed in previously reported work; and most critically, the stress level at which models tests are conducted. In small scale 1 g model tests, soil self-weight body forces are not scaled appropriately to prototype. Consequently, the disparity in stress level compared to full scale represents the greatest challenge to the ethos of transparent soil modelling and brings into question the validity of interpretations and conclusions drawn using this approach. This is a considerable

shortcoming of the current methodology and clearly it would be desirable if tests were conducted at more representative field stresses provided by either a calibration chamber whereby increased confining stresses could be applied, or in elevated gravity conditions produced by a centrifuge. In this respect, [Song et al. \(2009\)](#) investigated plate anchor embedment using transparent soil in the centrifuge for the purpose of visualizing the anchor trajectory to validate numerical and analytical models. While this is the first reported use of transparent soil in the centrifuge to visualize deformation behavior, similar limitations pertained to the earlier work of [Gill \(1999\)](#) and [Gill and Lehane \(2001\)](#), whereby soil displacements were observed by tracking the position of a single row of 3 mm diameter beads suspended in the soil during consolidation. Anchor drag tests were conducted at 100 g, thus the 3 mm targets beads were equivalent to a 0.3 m diameter inclusion in the soil at prototype scale. This would undoubtedly have an impact on the soil stress and strength regime, which was unquantified in the work, in addition to only offering coarse measurement resolution. Nevertheless, despite these shortcomings, the authors reported positive correlation with complementary analytical and numerical predictions, thus offering initial validation of transparent soils within the high gravity centrifuge environment.

This paper recognizes these limitations and outlines the development of improved testing methodology, whereby transparent soil in conjunction with laser aided imaging are translated to the centrifuge, thus benefiting from the elevated stress conditions provided when testing models in the high gravitation acceleration field but also offering higher measurement resolution capabilities associated with the laser aided DIC ([Fig. 2](#)).

FIG. 2 Inertial stress in a centrifuge model and corresponding prototype and the experimental concept of modelling of models.

This investigation is the first of its kind, thus the principle aims of this paper are to (i) describe the technical challenges associated with implementing this revised experimental methodology, (ii) summarize the test equipment/systems developed, and (iii) present preliminary experimental results to validate and confirm the successful implementation of transparent soil testing to the high gravity centrifuge test environment. A demonstration application of two shallow strip foundations is reported using the principle of “modelling of models” to confirm similitude at different scales (**Fig. 2**). The scientific developments discussed have the potential to provide a step change in transparent soil modelling methodology crucially by providing more representative stress levels that reflect prototype conditions, while making a broader positive contribution to physical modelling capabilities to assess complex soil–structure boundary problems.

Experimental Material and Preparation

TRANSPARENT SOIL MATERIAL

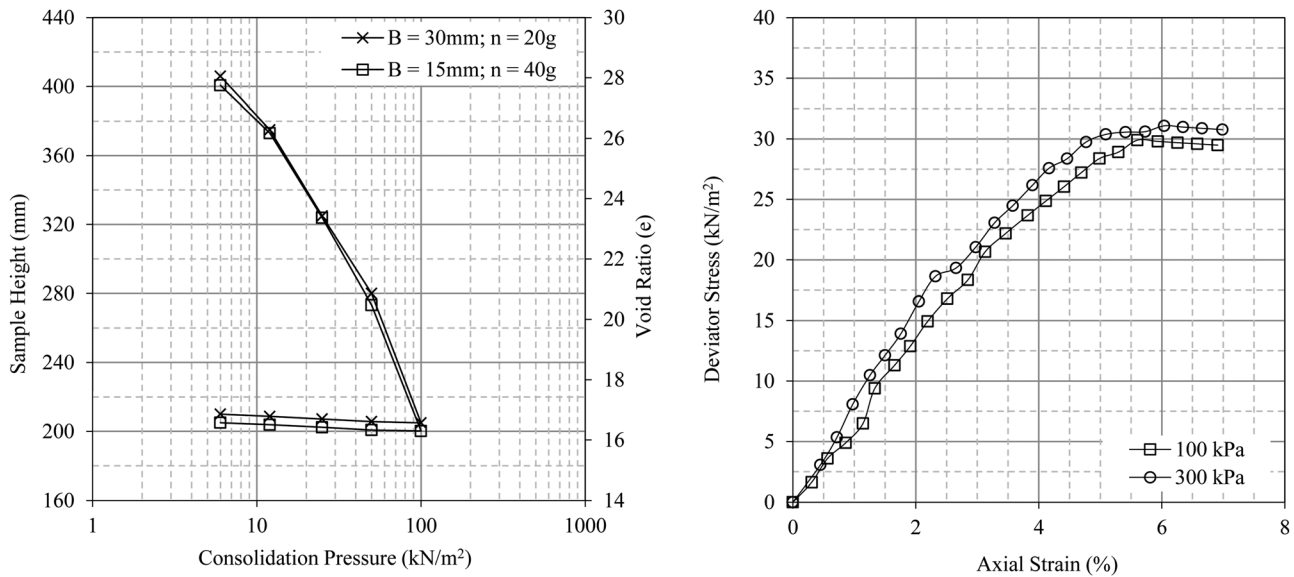
The transparent soil used in this investigation consisted of 6 % fumed amorphous silica aggregate and 94 % pore fluid. The pore fluid was a blend of white oil (Baylube WOM 15) and paraffinic solvent (N-paraffin C10-13) mixed to volumetric proportions of 77:23, giving a refractive index match to the silica aggregates of 1.467 at 20°C. This ratio was previously calibrated by [Stanier \(2011\)](#) using a visual eye chart assessment method; however, this approach was superseded by a newly established

quantitative framework proposed by [Black and Take \(2015\)](#) based on the principle of modulation transfer function.

The particle density of the fumed silica was 2200 kg/m³, surface area of 200 ± 25 m²/g, and particle size D₅₀ of 0.014 μm. The density of the fluids was measured to be 845.48 kg/m³ for Baylube WOM 15 and 764.24 kg/m³ for N-paraffin C10-13. The dynamic viscosity of the oils was measured using a spindle viscometer in units of centipoises (cP) and determined to be 21.2 cP and 1.2 for the Baylube and Paraffin oils, respectively, and 7.7 cP for the combined fluid mix ratio at 20°C.

SAMPLE PREPARATION

Fumed silica powder was blended with mixed oil pore fluid to form consistent soil slurry. Timiron seeding particles were added to half the slurry mixture and each batch was mixed thoroughly using a hand held food mixer. The addition of timiron powder was necessary to provide artificial texture within the soil that is visible under laser illumination. The slurry was de-aired to form a two phase material, which is a vital step as entrained air leads to a loss of transparency. The soil slurry was poured into the chamber with the aid of a split-mould. This enabled slurry seeded with timiron particles to be located in the rear of the model and the front section filled with slurry containing no timiron particles so as to provide optimal transparency to the plane of interest. The split mould was removed immediately once the soil slurry was poured prior to any applied consolidation stress in order to produce a vertical soil interface located 95 mm from the front of viewing window. This off-centre interface provided sufficient overlap to produce high quality seeding texture when the laser sheet is passed along the centreline of the chamber.

FIG. 3 Sample properties: (a) consolidation characteristics and (b) stress–strain behavior during undrained triaxial tests.

The slurry was then consolidated in stages of 6, 12, 25, 50, and 100 kN/m² to produce a sample of dimensions 200 by 200 mm. Two samples were produced for this investigation and the consolidation characteristics are shown in **Fig. 3**, which confirms a high degree of repeatability. At the final pressure increment, the coefficient of consolidation (c_v) and coefficient of compressibility (m_v) was 1.5 m²/year and 4.2 kN/m², respectively, which is consistent with other results quoted in literature (Iskander et al. 1994; Gill 1999; McKelvey 2002, Iskander et al. 2002a; Stanier 2011). Consolidated samples were transferred to the centrifuge for testing. During spin up and testing, drainage was prevented (i.e., undrained tests); thus no further consolidation occurred. Consolidated transparent soil has a unit weight of approximately 10 kN/m³; hence, for the soil bed model height of 200 mm tested at a gravity of 40 g, the soil self-weight total stress at the base of the model would be 80 kN/m². Therefore, given the undrained testing conditions and lower soil stress than that statically applied, no additional compression of the soil would have occurred as a result of the sample being prepared at 1 g but tested in the centrifuge.

A third sample was consolidated to the same effective stress of 100 kN/m² for the purpose of soil strength measurement. Triaxial tests were conducted on two 38 mm diameter specimens, extracted using sample tubes, at confining stresses of 100 and 300 kN/m². In both tests, the deviator stress at failure was approximately 30 kN/m², which yielded an undrained shear strength (c_u) of 15 kN/m² (**Fig. 3**). Soil stiffness and rigidity index were determined to be approximately 800 kN/m² (determined by the secant modulus) and 55, respectively.

Experimental Apparatus

CENTRIFUGE PLATFORM

The centrifuge used for this investigation was the newly established University of Sheffield 50 g-ton geotechnical beam centrifuge located in the Centre for Energy and Infrastructure Ground Research. The centrifuge was designed and manufactured by Thomas Broadbent and Sons Limited, United Kingdom, and commissioned in 2014. The centrifuge beam has a radius of 2 m to the base of the swing platform, of plan area 0.8 m², and can accelerate a 500 kg payload to 100 gravities. A summary of the technical specifications is presented in **Table 1** and a detailed overview of this facility provided in Black et al. (2014).

TABLE 1 Centrifuge specification and performance.

Description	Specification
Platform radius	2.0 m
Effective radius	1.7 m
Payload size	W = 0.8 m (circumferential) L = 0.8 m (vertical in flight) H = 0.9 m (radial in flight)
Maximum acceleration	500 kg at 100 g; 330 kg at 150 g
In-flight balancing capability	From a maximum ranging from ± 45 to ± 1.5 kN at 280 RPM
Hydraulic union	4-port, 10-bar g, 10°C–50°C
Slip ring: power	16-way 100 RMS at 40 A each
Slip ring: control	16-way 1000 RMS at 10 A each
Communication	Fiber optic rotary joint, multimode, rated 1000 RPM to 1 GB

TEST CHAMBER

Tests were performed in an aluminium chamber, fabricated from 20 mm thick plate, having internal dimensions of 200 by 200 by 560 mm. An extension collar was used to increase the height of the box to 800 mm, which facilitated homogenous beds to be reconstituted from slurry. The front panel of the main chamber was 20-mm thick Perspex, which provided a viewing window through which digital images were captured. Additional Perspex panels were integrated into the sides of the chamber to allow transmission of the laser light sheet to pass through the sample illuminating soil on the plane of interest along the centreline. The chamber was anodized black to absorb the laser light, which minimized backscatter and reflections into the model.

Once pre-consolidation was complete, the test chamber was removed from the static consolidation press and prepared for centrifuge testing. The chamber extension top collar was removed, drainage lines closed, and the sample transferred to the centrifuge platform. The test setup and configuration is discussed in more detail in the following sections.

LASER AIDED IMAGE SYSTEM—LASER MODULE

The advance of technology has led to the development of small form factor solid state laser modules that are considerably more compact than older generation air-cooled units. Nevertheless, despite this advance, there is always a great concern about the robustness and longevity of electronic components subjected to the high stresses imposed in the centrifuge environment. Implementation of a laser illumination source and optical lens configuration within this harsh stress environment is not a trivial matter and represents perhaps the biggest technical challenge to successfully implement transparent soil and DIC centrifuge based research. Several considerations in developing the laser illumination systems were (i) the laser output power required to illuminate the soil, (ii) physical geometry of the laser unit and power supply systems, (iii) the optical lens configuration needed to produce a uniform light sheet to illuminate the full height of the soil within the tight confines of the payload space available, and (iv) the impact of elevated stress on the internal laser components.

With respect to (i) and (ii), previous successful transparent soil modelling research at the University of Sheffield used a 1 W argon-ion air-cooled laser that produced a 0.95-mm diameter laser beam of 457–514 nm wavelength (λ). While the output power of this laser is sufficient to provide satisfactory illumination of soil texture, at 400 mm long, the laser unit is too large to be located in the centrifuge payload basket. An alternative solid state 2 W laser Opus 532 nm laser module was also available that offered a distinct advantage of being considerably smaller (165 by 115 by 50 mm). During initial conceptual designing of the experimental configuration, it was conceived that this laser could be located on the centrifuge platform in close proximity to the experimental test chamber. However, despite being rated

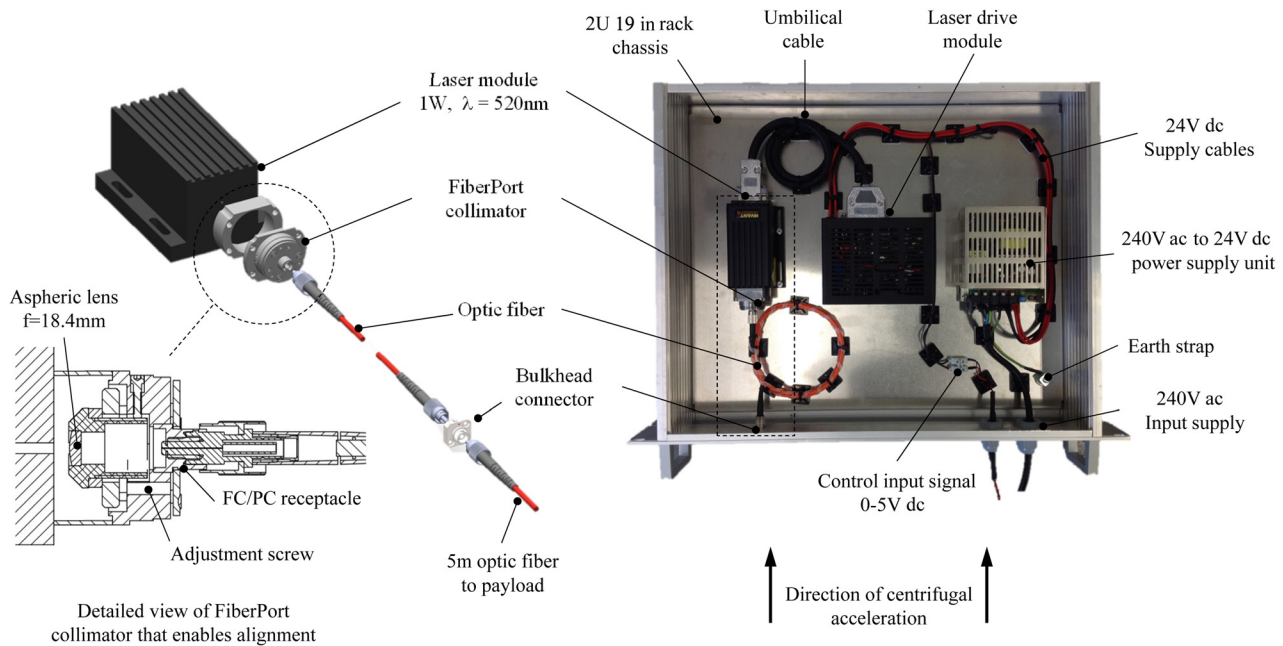
for a shock impact of 1200 g, discussion with the manufacturer about the orientation of the internal components revealed that fatigue may be a concern on sensitive diode mounting components during long-term stress exposure. Thus, it was clear that an alternative solution was necessary to minimize the risk of damaging or causing misalignment of the internal parts within the laser head.

Stress within the centrifuge environment is a function of the speed of rotation and radius from the centre of axis. While a permissible maximum operating gravity could be enforced to protect the laser components from high stress exposure, it was deemed that this would seriously restrict the potential of the technique. Therefore, to overcome difficulties associated with points (iii) and (iv) stated above, a novel approach was adopted whereby the laser module was mounted close to the centre of rotation with the laser light illumination distributed to the test package using a optic fiber delivery system. This concept was judged to be the most viable approach to address the previous concerns surrounding stress performance and available space on the centrifuge platform.

A new laser module was purchased specifically for use on the University of Sheffield centrifuge platform from Kvant Laser Systems UK. This unit consisted of a separate laser module rated 1 W at 520 nm wavelength and a drive board that enabled regulation of the laser output power using a 0–5 V dc input. The impact of vibration and increased stress on the laser module components are minimized internally by the use of zero-stress mounts, which eliminates mechanical strain within the head. The laser module and drive unit were mounted in the centrifuge data cabinets inside a standard 2U high 19 in. form factor chassis that was located at a radius of approximately 0.5 m from the centre of rotation (**Fig. 4**). Careful consideration was given to the orientation of the critical components such that the laser unit was positioned so that the centrifugal force acted axially in-line with the laser beam direction, as shown in **Fig. 4**. Mounting the laser head within the data cabinet significantly reduced the gravitational imposed stresses on the laser components. For example, a test at 60 g (assuming an effective radius of 1.7 m) is achieved at an angular velocity (ω) of 18.62 rad/s, which generates only 17 g at a radius of 0.5 m where the laser is located. The laser is powered by a variable 240 V ac power supply unit that produces a regulated 24 V dc to the drive board. Laser power is adjusted remotely from 0 to 1 W using a 0 to 5 V dc input control signal that is provided from the on-board National Instruments data acquisition system. Cables are passed through the front of the 19 in. rack mount chassis using PG9 cable glands.

LASER AIDED IMAGE SYSTEM—OPTIC FIBER DELIVERY SYSTEM

The optic fiber components are fully described in this section. Note, due to the considerable complexity of the experimental

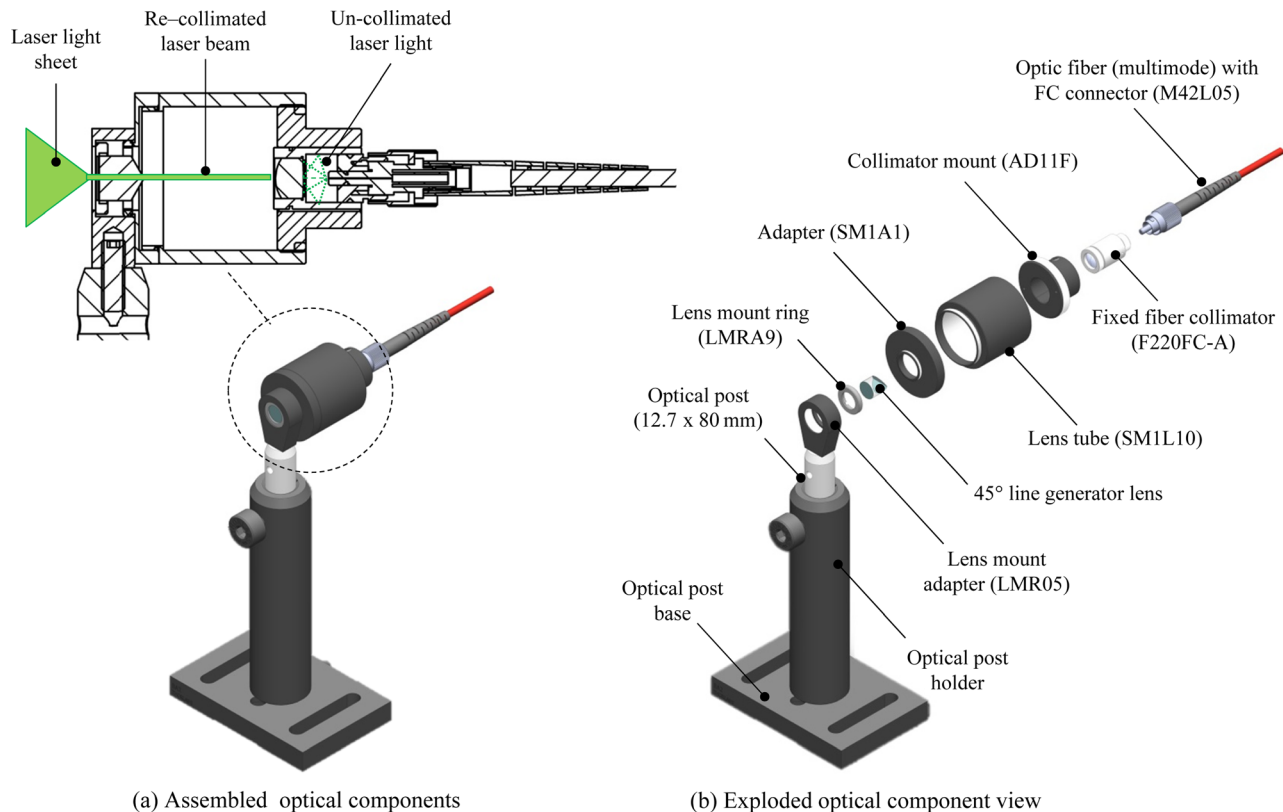
FIG. 4 Laser module and optic fiber system.

configuration, part numbers for individual components were identified and stated for information purposes of enabling other researchers to replicate and implement the optical arrangement described herein. The optical parts described were sourced from Thorlabs Inc.; however, it is possible to source similar items from a range of other leading suppliers of laser optical products.

The laser head was coupled with a FiberPort collimator (PAF-X-18-PC-A), mounted to the front face of the laser that enabled the laser beam to be directed into the optic fiber (Fig. 4). The collimator built-in aspheric lens can be aligned with 5 degree of freedom: linear alignment of the lens in the x and y , angular alignment for tip and tilt, and z adjustment using the tip and tilt controls simultaneously to enable precise alignment of the optical components. A laser intensity meter was used to precisely align the optics following which the locking setscrew were tightened to secure the lens position. A multi-mode (MM) fiber optic patch cable, of length 1 m (M42L01), having a $50 \mu\text{m}$ core and wavelength range 400 to 2400 nm, was mated with the FiberPort collimator. The MM patch cable was terminated with FC connectors and ceramic ferrules on both ends. Furcation tubing, 3 mm in diameter, protected the delicate internal optical fiber core from damage. The optic fiber inside the 19 in. laser chassis module was terminated at a FC/PC bulkhead connector (ADAFCPM2) on the front face of the chassis. This proved highly beneficial as it enabled the laser hardware to be easily removed from the centrifuge when not in use for transparent soil testing, which reduced unnecessary exposure to high gravity stresses.

A 5-m long MM fiber optic patch cable (M42L05) of the same specification was routed inside a 20-mm diameter corrugated flexible trunking from the data acquisition cabinet along the beam arm and toward the centrifuge payload. The fiber terminated into a pre-aligned fixed focus aspheric lens collimator to re-establish a high quality laser beam (Fig. 5). A fixed fiber collimator (F220FC-A) was chosen in this location, as unlike the FiberPort that was coupled with the laser, it had no movable parts; thus it was compact and would not be susceptible to misalignment from the higher stresses generated within the payload. It is well established that losses of up to 30 % (i.e., efficiency of only 70 %) can occur when using optic fiber coupled lasers owing to alignment errors and internal losses within the fiber itself. The efficiency achieved in the current optical fiber delivery system was 90 %, such that the laser yielded an output power of 0.97 W without a fiber attached and 0.87 W with the fiber connected. This high level of efficiency was achieved through careful selection of optical components; for example (i) selecting MM patch cable as it allows for more light at a greater range of spatial frequencies to enter the fiber due to the larger core size compared to single mode (SM) fiber, (ii) MM cable is preferred to SM cable as it is easier to couple, align, and focus the laser light onto the larger target (core size) exposed, and (iii) ensuring that the optical lens components are compatible with the fiber and they have a suitably large numerical aperture (NA) to ensure that the light exiting the fiber will be collected by the lens for collimation. The fixed fiber collimator (F220FC-A) attached to the end of the fiber in this experimental

FIG. 5 Optic lens assembly within the centrifuge payload. (a) assembled optical components and (b) exploded optical component view.



configuration had a numerical aperture of 0.22, which was similar to the M42L multimode fiber optic cable.

The optic fiber delivery system proved highly successful to produce a re-collimated laser beam of light at the payload area for testing. Considerable benefits of this system were that it removed the necessity for the laser head to be located in the highest stress field and also served to minimize the footprint of the optical components in the payload volume. Similar to previous laser aided transparent soil model tests conducted at 1 g, it was necessary to transform the laser beam into a light sheet to illuminate a vertical plane of interest within the model. This was achieved using a 45° optical lens that transformed the laser beam into a sheet of light of uniform intensity (Fig. 5). The lens was fixed to a stainless steel optical lens mount ring (LMRA9), which in turn was located inside a 12.7 mm lens mount adapter (LMR05), and interfaced with a threaded adapter (SM1A1), lens tube (SM1L10), and collimator mounting adapter (AD11F). The optical assembly was mounted on a 12.7 mm diameter lens post that provided height adjustment of the light sheet and was supported by a suitable post holder and base plate.

CAMERA SETUP

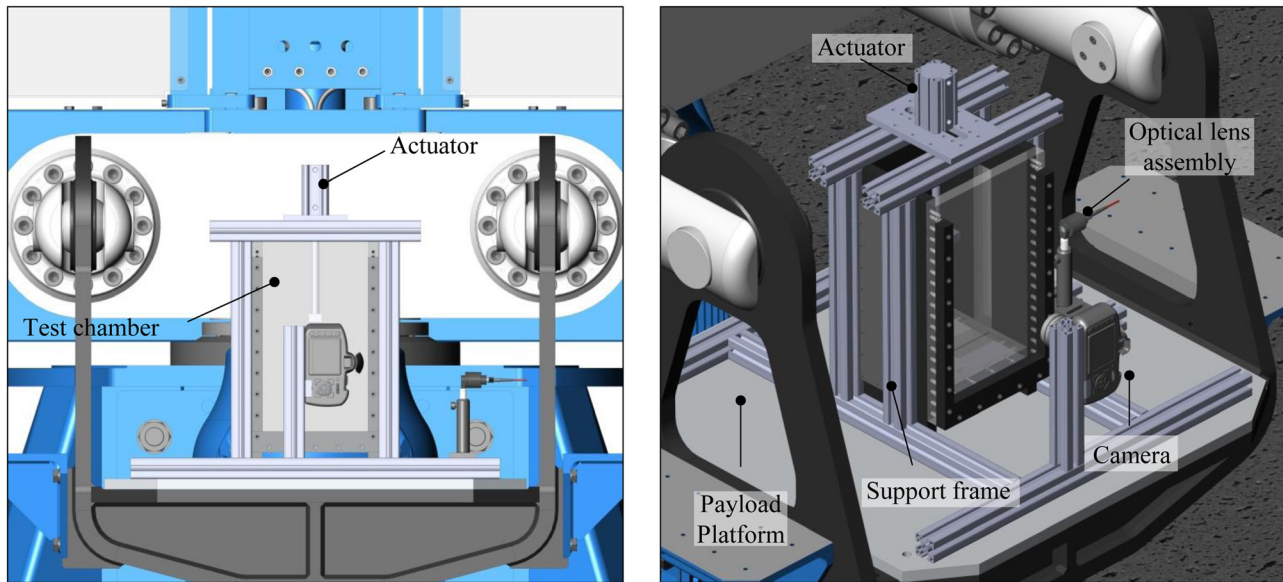
Images were captured using a Canon EOS 1100D Single Lens Reflex (SLR) with an 18-55 mm lens. The camera was

ruggedized by a support framework, located at a distance of 0.5 m from the front of the test chamber, and was triggered at regular intervals using a digital signal generated from the National Instruments data acquisition device. This remote trigger capability ensured that it was possible to initiate the camera to capture images prior to commencing the footing loading. The camera properties were fixed at focal length of 18 mm, an aperture of F/16, shutter speed of 1/10th s, ISO of 100, and no flash. These parameters were optimized prior to commencing the main test schedule to yield the greatest clarity of the timiron soil texture on the viewing plane. Images were taken at a rate of 3 frames per second (fps) during the foundation loading. These rigorous precautions ensured that the soil texture would be well-distinguished and therefore yield a high level of tracking capability.

Test Setup and Procedure

A conceptual 3D model was developed of the proposed experimental test arrangement to confirm the position of each element within the centrifuge payload basket (Fig. 6) and to enable greater visualization of the working area for the laser optical assembly. The actual payload package developed using this conceptual model is shown in Fig. 7. The test chamber was

FIG. 6 Test configuration proposed for transparent soil modelling in the centrifuge payload.



mounted and secured to the centrifuge platform using industrial grade 40 by 40 mm extruded aluminum profile, which in turn enabled fixing of the camera and optical assembly components. The optical lens was aligned, with the laser at low power while wearing suitable eye protection, to penetrate the along the center line of the test chamber ensuring that it illuminated the entire soil height. During testing, the laser output was set to full power as this was pre-determined to provide the optimum illumination of the soil texture to minimize errors during image correlation process. Images of the sample under laser illumination are shown in Fig. 8.

Two model strip footings of width (B) 15 and 30 mm were fabricated from aluminum and sprayed matt black to minimize laser reflections. The footings were loaded using a 50 mm internal diameter double acting hydraulic actuator that was capable of producing 1 kN vertical force, and a stroke length of 50 mm that was more than sufficient to bring each footing to failure. The applied load and displacement were recorded using a load cell and linear variable differential transducer. Prior to spin up, the footing was positioned on the soil surface and locked in position with an upward vertical stress applied to the bottom of the actuator. The upward stress was necessary to balance the

FIG. 7 Transparent soil centrifuge test package.

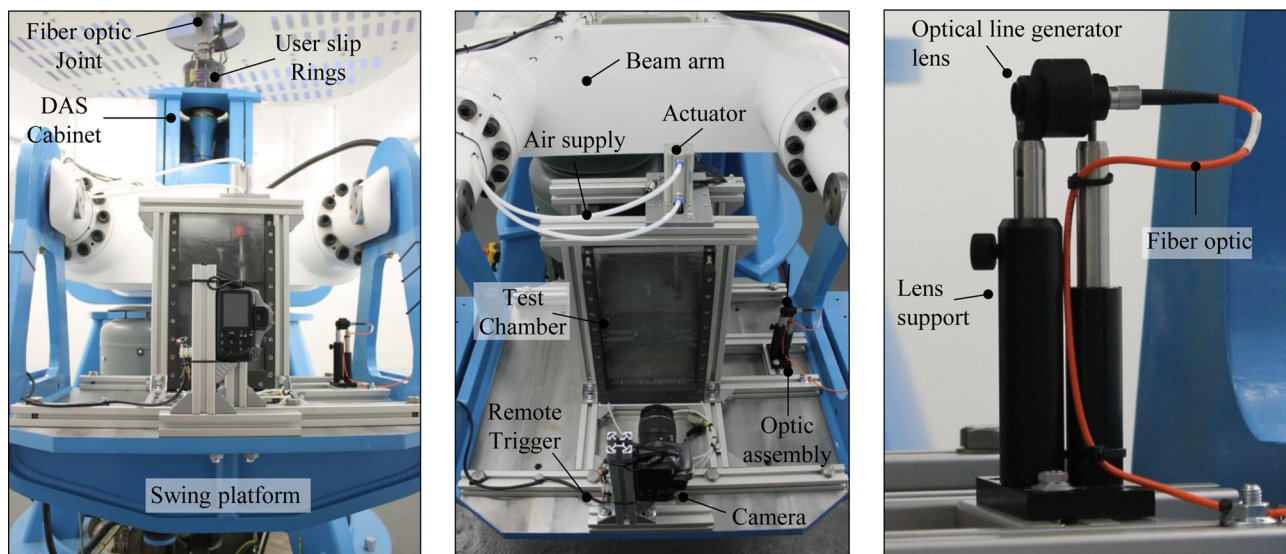
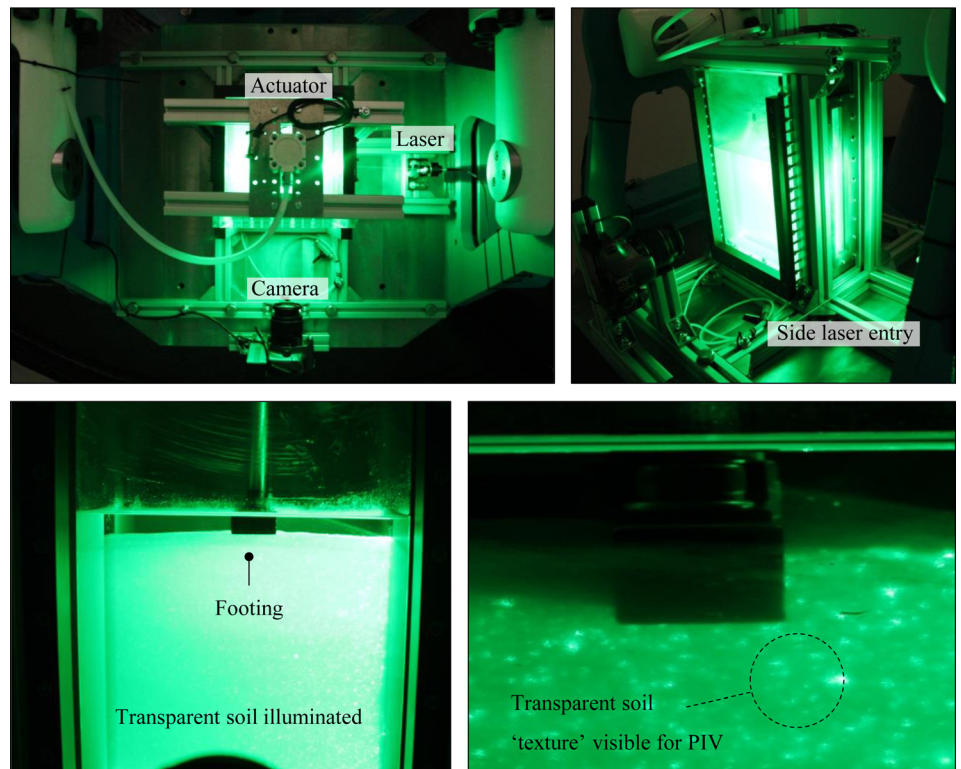


FIG. 8

Transparent soil centrifuge test package under laser illumination.



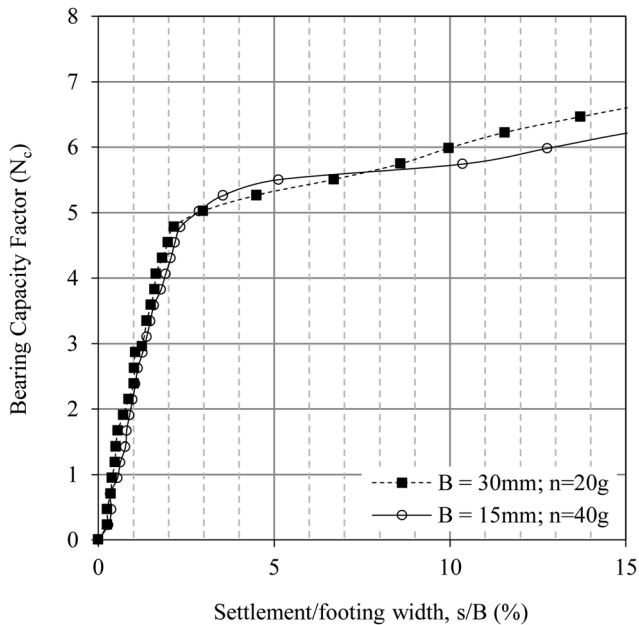
downward self-weight force of the footing load cell and connecting rods in the elevated gravity field to prevent premature penetration of the footing into the soil during spin up. The footing was loaded under stress control in a ramped mode by increasing the applied downward stress at a rate of 10 kN/m^2 per min until failure was observed, during which images were captured for DIC analysis. The rate of foundation penetration was determined to be approximately 0.012 mm/s and was sufficient to ensure a dimensionless velocity (vB/c_v) in excess of 30, ensuring undrained conditions were maintained during the loading phase (Finnie and Randolph 1994).

It is also worth noting that this fast loading rate was advantageous to mitigate changes in the ambient temperature at which the experiments were conducted. Black and Take (2015) and Black and Tatari (2015) demonstrated that changes in temperature affect the refractive index of transparent soil and consequently reduce its visual acuity. Current state-of-the-art transparent soil tests are conducted at 1 g in temperature-controlled laboratories whereby the model temperature and ambient room temperature are carefully controlled and maintained. In the newly developed experimental paradigm, the centrifuge containment chamber is the “laboratory environment” and susceptible to temporal changes in temperature during tests owing to the heat generated from the high power ac drive motor. Nevertheless, in the current investigation, tests

were completed in several minutes, not hours; thus potential detrimental temperature effects would be minimal. Review of the image series confirmed that no significant detrimental effects occurred in this instance; however, this may be a significant consideration in future research if longer test runs are needed such that it may necessitate the development of an environmental controlled chamber in which the test are conducted.

TESTING CONCEPT: MODEL OF MODELS

Scaling laws derive from the basic need to ensure stress similarity between the model and corresponding prototype. The concept of “modelling of models” involves testing a model of the same prototype at different scales to evaluate the impact of scaling variables on the applicability of the model configuration to represent the prototype. Similar results and observations from modelling of model tests are expected, which indicates the modelling conditions are not significantly influencing the scaling laws. The behavior of transparent soil at various scales is unknown; thus a key aspect to verify as part of this study was that the material exhibited similar behavior and was not adversely affected by varying scale conditions. For this purpose, a prototype strip foundation problem of width 0.6 m was chosen to be represented by model footing tests of width 15 and 30 mm , tested at 40 and 20 g , respectively, as previously shown in Fig. 2. The horizontal boundary conditions in each test from

FIG. 9 Normalized foundation response during loading.

the centerline of the footing were $6.6B$ and $3.3B$, which were deemed acceptable to avoid significant boundary effects.

Results and Discussion

Following each footing test, the load and settlement recorded during installation were converted to prototype units. The load deflection response for each model of the prototype is shown in **Fig. 9**. The installation resistance was normalized with respect to the undrained soil strength determined from the complementary triaxial tests ($c_u = 15 \text{ kN/m}^2$) and plotted as the dimensionless parameter of bearing capacity factor (N_c); footing settlement (s) is normalized with respect to the prototype foundation width (i.e., s/B).

From initial inspection of the installation behavior, it is evident that a similar global footing response is achieved from the two independent tests conducted of the same prototype problem. This observation provides confidence that transparent soil can be used as a viable modelling material in centrifuge tests as the same phenomenon is observed at two different model scales. The initial installation response is linear up to approximately $s/B = 2.5\%$, beyond which the foundation penetrates and reaches its ultimate capacity. The bearing capacity factor for each was determined to be approximately 5.2 to 5.3, which compares favorably with classic undrained bearing capacity theory proposed by [Prandtl \(1921\)](#) and [Skempton \(1951\)](#) for a strip footing on a purely cohesive soil. The aforementioned authors postulated a bearing capacity factor of 5.14 for an infinite strip foundation resting on the soil surface, having smooth footing interface and saturated homogeneous weightless clay

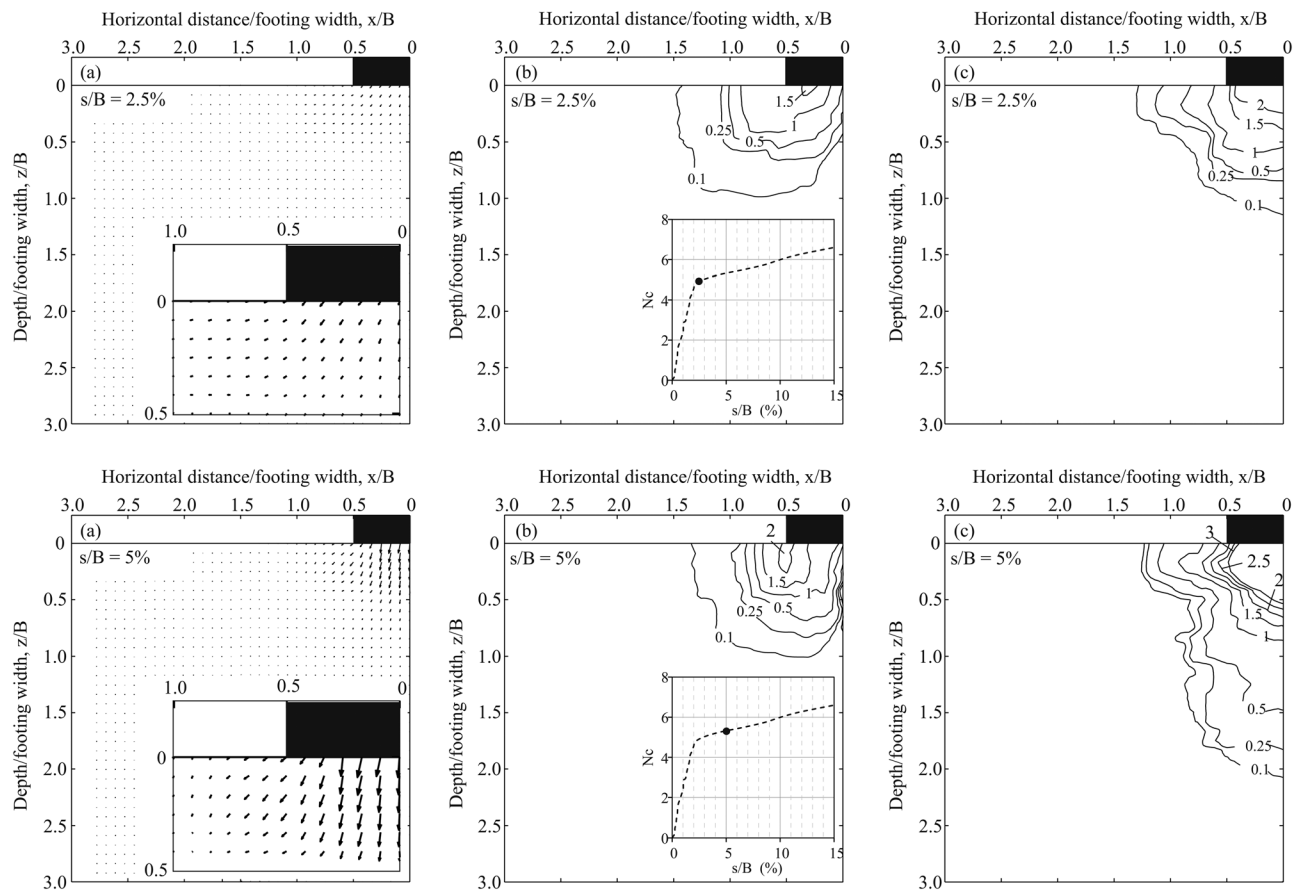
soil, with correction factors provided to account for embedment depth and footing geometry. The present work verifies this well-established theory, with only minimal variation observed, which provides further confidence of the ability of transparent soil to successfully deliver realistic kinematic soil behavior similar to prototype.

As the foundation penetrates further into the soil, $s/B > 5\%$, some continued increase in bearing capacity is observed. This gradual increase is likely to be caused by the footing mobilizing additional resistance as it penetrated deeper into the underlying soil and also a contribution of the increased soil stress with depth ([Davis and Booker 1973](#)) that generated in the elevated gravity field. A further possible reason for the slightly increased bearing capacity in the model tests could be due to the additional resistance generated along the interfaces of the foundation as it displaces into the soil. Additional side, end, and bottom friction resistance are not accounted for within simple bearing capacity theory of [Prandtl \(1921\)](#) and [Skempton \(1951\)](#), which would result in slightly increased bearing capacity factors as widely reported by authors such as [Terzaghi \(1943\)](#) and [Meyerhof \(1963\)](#).

Soil–structure interaction deformation behavior is discussed with reference to the 30 mm footing tested at 20 g and depicted in **Fig. 10**. Similar observations regarding the extent and magnitude of the displacement pattern were also observed in the 15 mm footing at 40 g. Image analysis was conducted using GeoPIV ([White et al. 2003](#)) at a 50 pixel patch size that yielded a standard error of 0.008 pixels, which is comparable to the precision quoted by [White et al. \(2003\)](#) and other 1 g transparent soil work reported by [Stanier et al. \(2012\)](#). Prior to conducting the main footing tests, the image processing methodology was optimized to account for lens distortion and internal refraction between the control plane containing the stationary fixed control points and the viewing plane illuminated by the laser light sheet. Further in-depth discussion of calibration and error mitigation when using transparent soil can be found in [Stanier et al. \(2012\)](#). **Figure 10** presents the soil vector displacement component beneath the footing during the application of load, and the horizontal and vertical prototype soil displacement contours normalized with respect to the prototype footing width at relative strain of $s/B = 2.5\%$ and 5% .

At $s/B = 2.5\%$, the zone of influence of soil displacement extends up to approximately $x/B = 1.5$ and $z/B = 1.0$. The extent to which the soil is affected by the foundation penetration remains similar as the soil yields and fails up to $s/B = 5\%$. As expected, greater magnitudes of displacement are observed closer to the footing where the applied stress is highest; for example, at $s/B = 2.5\%$, a small region of 1.5% normalized horizontal displacement is observed directly beneath the footing. As the foundation approaches ultimate limit state (ULS) (i.e., $s/B = 5\%$) the magnitude of horizontal displacement increases to 2 along the edge of the penetrating footing, with a visible

FIG. 10 Soil structure interaction response for footing test B = 30 mm at 20 g; (a) vector plot, (b) horizontal strain contour, and (c) vertical strain contour at a footing strain of $s/B = 2.5$ and 5 %.



increase in the zone of the 1 and 1.5 displacements contours. This observation of horizontal displacements occurring in contact with the footing is very interesting as ordinarily, the horizontal displacement immediately beneath the centre of the footing would be expected to be zero, i.e., frictionless. This indicates that some interface friction would be generated along the soil–structure interface, which could have contributed to the slightly higher bearing capacity factors observed, as reported by Meyerhof (1963) and Vesic (1973). Examination of Fig. 8 (lower left image) reveals that the soil surface may not have been perfectly flat but curved owing to the soil swelling and the sides being restrained along the chamber walls. This could have caused small variations in the initial contact condition between the soil and the footing which may have initiated and contributed to the observed horizontal displacement beneath the footing.

The vertical soil displacement behavior is also presented in Fig. 10 for the 30 mm wide footing. Similar to the horizontal displacements, the largest soil deformation occurred in close proximity to the foundation and diminished with increasing distance from the source of applied load. At $s/B = 2.5$ %, up to 2 % normalized vertical displacement is observed directly

beneath the footing, which reduces progressively to 0.1 at $x/B = 1.25$ and $z/B = 1.0$. As s/B increases to 5 %, the normalized vertical displacement immediately in contact with the foundation increases; however, a more evident change is the increase in the extent to which soil movement occurs directly below the footprint of the foundation. The zone of influence increases from $x/B = 1.0$ to 2.0, while the horizontal displacements remain relatively unchanged. This is a clear indication that the foundation has failed and is penetrating excessively into the soil and the extent of deformation and the plastic zone is consistent with that observed in similar shallow footing tests reported O’loughlin and Lehane (2009) and Leung et al. (1984). Nevertheless, it is also clear that the boundary conditions provided in the test were suitable as the displacement contours remained contained in the soil and well away from the chamber boundaries.

Conclusions

Transparent soils have enabled internal visualization of geotechnical processes in physical models. While developments have been made to enhance the methodology of the modelling

technique, low stress conditions provided in small 1 g model tests remains a considerable limitation to the approach and raises uncertainty in conclusions drawn from observations obtained using this method. This paper reported on the development of an improved experimental methodology, whereby transparent soil and laser aided imaging are translated to the centrifuge environment. The paper described the technical challenges associated with implementing this approach and fully documented the test equipment/systems developed. The modelling approach was validated using a 0.6 m wide prototype strip foundation problem at two length scales, tested at 20 and 40 g, using the principle of “modelling of models.” Similar load–displacement response is observed in both tests, which yielded bearing capacity factors in good agreement with classical bearing capacity theory. The laser aided imaging technique proved highly successful and enabled observation of detailed soil–structure interaction failure mechanics. The modelling of model tests confirmed the viability of transparent soil to be successfully implemented in the centrifuge test environment. The experimental developments presented provide a step change in transparent soil modelling methodology and offer potential for contributing greater scientific understanding complex soil–structure boundary problems.

ACKNOWLEDGMENTS

Funding support provided by the Engineering Physical Sciences Research Council (EPSRC) to establish the 2 m diameter beam centrifuge and Centre for Energy and Infrastructure Ground Research at the University of Sheffield is gratefully acknowledged (EP/K040316/1). Continued technical support by Neil Baker and Alan Ainsworth, Thomas Broadbent and Son Ltd. is acknowledged. This work was supported by the expertise of the Department of Civil & Structural Engineering technical staff, Paul Osborne, Mark Foster, Alex Cargill, Dave Callaghan, Paul Bentley (Electronics), and Alan Grundy (IT) for in-house fabrication of centrifuge systems and supporting its operation. Support from Martin Pelikan of Kvant Laser Systems UK, and Mike Souby of Thorlabs Ltd for the technical support offer regarding the specification of the laser optic fiber components is also acknowledged.

References

- Ahmed, M. and Iskander, M., 2010, “Analysis of Tunnelling Induced Ground Movements Using Transparent Soil Models,” *J. Geotech. Geoenviron. Eng.*, Vol 137, No. 5, pp. 525–535.
- Andrawes, K. and Butterfield, R., 1973, “The Measurement of Planar Displacements of Sand Grains,” *Geotechnique*, Vol. 23, No. 5, pp. 571–576.
- Black, J. A., 2012a, “Ground displacement during press-in piling using transparent soil and PIV,” *Proceedings of the International Press-In Association, 4th IPA Workshop*, Singapore, Dec 6–7, International Press-In Association, Tokyo, Japan, pp. 1–8.
- Black, J. A., 2012b, “Soil Sample Disturbance During Site Investigation,” *Technical Report to Environmental Scientifics Group—Geotechnical Services Division*, Environmental Scientifics Group, Burton, UK.
- Black, J. A., Baker, N., and Ainsworth, A., 2014, “Establishing a 50 g-Ton Geotechnical Centrifuge at the University of Sheffield,” *Proceedings of the 8th International Conference on Physical Modelling in Geotechnics*, Perth, Australia, Jan 14–17, C. Gaudin and D. White, Eds., CRC Press, Boca Raton, FL, pp. 181–186.
- Black, J. A. and Take, W., 2015, “A Framework for Assessing Optical Quality of Transparent Soil,” *ASCE Geotech. Test. J.* (submitted).
- Black, J. A. and Tatari, A., 2015, “Transparent Soil to Model Thermal Processes: A Thermal Pile Example,” *ASCE Geotech. Test. J.* (submitted).
- Butterfield, R., Harkness, R., and Andrawes, K., 1970, “A Stereo-Photogrammetric Method for Measuring Displacement Fields,” *Geotechnique*, Vol. 20, No. 3, pp. 308–314.
- Davis, E. H. and Booker, J. R., 1973, “The Effect of Increasing Strength With Depth on the Bearing Capacity of Clays,” *Geotechnique*, Vol. 23, No. 3, pp. 551–563.
- Finnie, I. M. S. and Randolph, M. F., 1994, “Punch-Through and Liquefaction Induced Failure of Shallow Foundations on Calcareous Sediments,” *Proceedings of the 7th International Conference on Behaviour of Offshore Structures*, Boston, MA, July 12–15, Pergamon Press, London, pp. 217–230.
- Forlati, G. and Black, J. A., 2014, “Impact of Pile Geometry on the Installation of Open Ended Press-In Piles,” *Proceedings of the 8th International Conference on Physical Modelling in Geotechnics*, Perth, Australia, Jan 14–17, C. Gaudin and D. White, Eds., CRC Press, Boca Raton, FL, pp. 763–769.
- Gill, D. and Lehane, B., 2001, “An Optical Technique for Investigating Soil Displacement Patterns,” *Geotech. Test. J.*, Vol. 24, No. 3, pp. 324–329.
- Gill, D., 1999, “Experimental and Theoretical Investigations of Pile and Penetrometer Installation in Clay,” Ph.D. thesis, Trinity College, Dublin, Ireland.
- Hird, C., Ni, Q., and Guymer, I., 2008, “Physical Modelling of Displacements Around Continuous Augers in Clay,” *Foundations: Proceedings of the 2nd British Geotechnical Association International Conference on Foundations*, Dundee, UK, June 24–27, J. Knappett, Ed., Vol. 1, IHS BRE Press, Englewood, CO, pp. 565–574.
- Iskander, M., 2010, *Modelling With Transparent Soils: Visualizing Soil Structure Interaction and Multi Phase Flow, Non-Intrusively*, Springer, New York.
- Iskander, M., Lai, J., Oswald, C., and Mannheimer, R., 1994, “Development of a Transparent Material to Model the Geotechnical Properties of Soils,” *ASCE Geotech. Test. J.*, Vol. 17, No. 4, pp. 425–433.
- Iskander, M. and Liu, J., 2010, “Spatial Deformation Measurement Using Transparent Soil,” *ASCE Geotech. Test. J.*, Vol. 33, No. 4, pp. 314–321.
- Iskander, M., Lui, J., and Sadek, S., 2002a, “Transparent Amorphous Silica to Model Clay,” *ASCE Geotech. Test. J.*, Vol. 128, No. 3, pp. 262–273.
- Iskander, M., Sadek, S., and Lui, J., 2002b, “Optical Measurement of Deformation Using Transparent Silica Gel to Model

- Sand," *Int. J. Phys. Modell. Geotech.*, Vol. 2, No. 4, pp. 27–40.
- Kelly, P., 2013, "Soil Structure Interaction and Group Mechanics of Vibrated Stone Column Foundations," Ph.D. thesis, University of Sheffield, Sheffield, UK.
- Leung, P. K., Schiffman, R. L., Ko, H. Y., and Pane, V., 1984, "Centrifuge Modelling of Shallow Foundation on Soft Soil," *Proc. 16th Offshore Technology Conference* 3, pp. 275–282.
- Liu, J., Iskander, M., and Sadek, S., 2002, "Optical Measurement of Deformation Under Foundations Using a Transparent Soil Model," *International Conference on Physical Modelling in Geotechnics: ICPMG*, St. Johns, Newfoundland, Canada, July 10–12, R. Phillips, P. J. Guo and R. Popescu, Eds., Taylor & Francis, London, pp. 155–159.
- McKelvey, D., 2002, "The Performance of Vibro Stone Column Reinforced Foundations in Deep Soft Ground," Ph.D. thesis, Queens University, Belfast, UK.
- McKelvey, D., Sivakumar, V., Bell, A., and Graham, J., 2004, "Modelling Vibrated Stone Columns in Soft Clay," *Proc. Inst. Civ. Eng.: Geotech. Eng.*, Vol. 157, No. 3, pp. 137–149.
- Meyerhof, G. G., 1963, "Some Recent Research on the Bearing Capacity of Foundations," *Can. Geotech. J.*, Vol. 1, No. 1, pp. 16–26.
- O'Loughlin, C. D. and Lehane, B. M., 2009, "Nonlinear Cone Penetration Test-Based Method for Predicting Footing Settlements on Sand," *ASCE Geotech. Geoenviron. Eng.*, Vol. 136, No. 3, pp. 409–416.
- Prandtl, L., 1921, "On the Penetrating Strengths (Hardness) of Plastic Construction Materials and the Strength of Cutting Edges," *Z. Angew. Math. Mech.*, Vol. 1, No. 1, pp. 15–20 (in German).
- Sadek, S., Iskander, M., and Lui, J., 2002, "Geotechnical Properties of Transparent Silica," *Can. Geotech. J.*, Vol. 39, No. 1, pp. 111–124.
- Sadek, S., Iskander, M., and Lui, J., 2003, "Accuracy of Digital Image Correlation for Measuring Deformations in Transparent Media," *ASCE J. Comput. Civ. Eng.*, Vol. 17, No. 2, pp. 88–96.
- Skempton, A. W., 1951, "The Bearing Capacity of Clays," *Build. Res. Congr.*, Vol. 1, 1951, pp. 180–189.
- Song, Z., Hu, Y., O'Loughlin, C., and Randolph, M., 2009, "Loss in Anchor Embedment During Plate Anchor Keying in Clay," *ASCE J. Geotech. Geoenviron. Eng.*, Vol. 135, No. 10, pp. 1475–1485.
- Stanier, S. A., 2011, "Modelling the Behaviour of Helical Screw Piles," Ph.D. thesis, University of Sheffield, Sheffield, UK.
- Stanier, S. A., Black, J. A., and Hird, C. C., 2012, "Enhancing Accuracy and Precision of Transparent Synthetic Soil Modelling," *Int. J. Phys. Modell. Geotech.*, Vol. 12, No. 4, pp. 162–175.
- Stanier, S. A., Black, J. A., and Hird, C. C., 2013, "Modelling Helical Screw Piles in Clay and Design Implications," *Proc. Inst. Civ. Eng.: Geotech. Eng.* (available online).
- Taylor, R. N., Grant, R. J., Robson, S., and Kuwano, J., 1998, "An Image Analysis System for Determining Plane and 3-D Displacements in Soil Models," *Proceedings of the International Conference Centrifuge 98*, Tokyo, Japan, Sept 23–25, Taylor & Francis, London, pp. 73–78.
- Terzaghi, K., 1943, *Theoretical Soil Mechanics*, Wiley, New York.
- Vesic, A. S., 1973, "Analysis of Ultimate Loads of Shallow Foundations," *ASCE J. Soil Mech. Found. Div.*, Vol. 99, No. 1, pp. 45–73.
- White, D., Take, W., and Bolton, M., 2003, "Soil Deformation Measurement Using Particle Image Velocimetry (PIV) and Photogrammetry," *Geotechnique*, Vol. 53, No. 7, pp. 619–631.